Materials Today Bio 16 (2022) 100286

Contents lists available at ScienceDirect

Materials Today Bio

journal homepage: www.journals.elsevier.com/materials-today-bio

Carbon dots conjugated to SN38 for improved colorectal anticancer therapy

Deborah Mattinzoli [a,1,**], Michele Cacioppo [b,c,1,2], Masami Ikehata [a], Silvia Armelloni [a], Carlo Maria Alfieri [d,e,***], Giuseppe Castellano [d,e], Mario Barilani [f,g], Francesca Arcudi [b,3,****], Piergiorgio Messa [d,e], Maurizio Prato [b,c,h,*]

[a] Renal Research Laboratory, Fondazione IRCCS Ca' Granda Ospedale Maggiore Policlinico, Via Pace 9, Milan, 20122, Italy
[b] Department of Chemical and Pharmaceutical Sciences, INSTM UdR Trieste, University of Trieste, Via Licio Giorgieri 1, Trieste, 34127, Italy
[c] Center for Cooperative Research in Biomaterials (CIC BiomaGUNE), Basque Research and Technology Alliance (BRTA), Paseo de Miramón 182, Donostia-San Sebastián, 20014, Spain
[d] Unit of Nephrology, Dialysis and Renal Transplant Fondazione IRCCS Ca' Granda Ospedale Maggiore Policlinico, Via Della Commenda 15, Milan, 20122, Italy
[e] University of Study of Milan, Via Festa Del Perdono 7, 20122, Milan, Italy
[f] EPIGET LAB, Department of Clinical Sciences and Community Health, University of Milan, Milan, 20122, Italy
[g] Department of Transfusion Medicine and Hematology, Cell Factory, Regenerative Medicine Laboratory, Fondazione IRCCS Ca' Granda Ospedale Maggiore Policlinico, Milan, 20122, Italy
[h] Ikerbasque, Basque Foundation for Science, Bilbao, 48013, Spain

ARTICLE INFO

Keywords:
Carbon dots
Colorectal cancer therapy
Drug delivery
SN38
Cell cycle
Extracellular matrix

ABSTRACT

Irinotecan (CTP-11) is one of the standard therapies for colorectal cancer (CRC). CTP-11 is enzymatically converted to the hydrophobic 7-ethyl-10-hydroxycamptothecin (SN38), a one hundred-fold more active metabolite. Conjugation of hydrophobic anticancer drugs to nanomaterials is a strategy to improve their solubility, efficacy, and selectivity. Carbon dots (CDs) have garnered interest for their small sizes (<10 nm), low toxicity, high water solubility, and bright fluorescence. This paper describes the use of CDs to improve drug vehiculation, stability, and chemotherapeutic efficiency of SN38 through a direct intracellular uptake in CRC. The covalent conjugation of SN38 to CDs via a carbamate bond provides a CD-SN38 hybrid material for slow, sustained, and pH-responsive drug release. CD-SN38 successfully penetrates the CRC cells with a release in the nucleus affecting first the cell cycle and then the cytoskeleton. Moreover, CD-SN38 leads to a deregulation of the extracellular matrix (ECM), one of the major components of the cancer niche considered a possible target therapy for reducing the cancer progression. This work shows the combined therapeutic and imaging potential of CD-based hybrid materials for the treatment of CRC. Future efforts for targeted therapy of chronic diseases characterized by altered ECM deposition, such as chronic kidney disease and chronic allograft nephropathy in kidney transplant patients are envisaged.

Abbreviations: CNDs, carbon nanodots; CD-SN38, CNDs conjugate with SN38; CDK7, cyclin-dependent kinase 7; COLIαI, collagen type I alpha 1 chain; CRC, colorectal cancer; CPT11, camptotecin 11; o.n., overnight; ECM, Extracellular Matrix; FBS, fetal bovine serum; FCS, fetal calf serum; HT29, CRC cell line; Ki-67, antigen Ki-67; HciGEnC, conditionally immortalized human glomerular endothelial cells; HciPodo, conditionally immortalized human podocytes; IF, immunofluorescence; LD50, 50% lethal dose; MTT, 3-[4,5-dimethylthiazol-2-yl]-2,5- diphenyltetrazolium bromide; PBS, phosphate buffer saline; RPL4, Ribosomal Protein L4; RT, room temperature; SD, standard deviation; SN38, 7-etil-10-idrossi-camptotecina; TGFβ1, transforming growth factor beta1; TME, Tumor Micro Environment; TNFα, tumor necrosis factor alpha.

* Corresponding author. Department of Chemical and Pharmaceutical Sciences, INSTM UdR Trieste, University of Trieste, via Licio Giorgieri 1, Trieste, 34127, Italy.
** Corresponding author.
*** Corresponding author. University of Study of Milan, via Festa Del Perdono 7, 20122, Milan, Italy.
**** Corresponding author.
E-mail addresses: deborah.mattinzoli@policlinico.mi.it (D. Mattinzoli), carlo.alfieri@policlinico.mi.it (C.M. Alfieri), francescarcudi@gmail.com (F. Arcudi), prato@units.it (M. Prato).
[1] Deborah Mattinzoli and Michele Cacioppo contributed equally to this work.
[2] Co-first author.
[3] Department of Chemistry, Northwestern University, 2145 Sheridan Road, Evanston, Illinois 60 208, USA.

https://doi.org/10.1016/j.mtbio.2022.100286
Received 26 January 2022; Received in revised form 30 April 2022; Accepted 9 May 2022
Available online 1 September 2022

1. Introduction

With high mortality (56%) and very low early detection rate (<39%), due to its asymptomatic condition, colorectal cancer (CRC) is considered the third most common human malignancy [1]. Little improvement in survival rate was observed only in the last decade due to the availability of more sensitive diagnostic investigation, less invasive surgical approaches, and improved chemotherapeutical tools [2]. One of the standard therapies for CRC is irinotecan (CPT-11), a semisynthetic derivative of the natural camptothecin (CPT), and commonly used either alone or in combination with other drugs (such as 5-fluorouracil or oxaliplatin) [3]. The pharmacological mechanism of CTP-11 is based on the inhibition of the topoisomerase I, which is a nuclear enzyme that plays a critical role in DNA replication and transcription [4]. Although CPT-11 exhibits itself an anticancer activity, it is mostly considered a prodrug because releases the SN38 derivative after metabolization that has an anticancer activity 100–1000 times higher than CPT-11 [5]. However the use of SN38 as an active anti-cancer metabolite is strongly dampened by its slow, incomplete and variable hydrolyzation, and its high hydrophobicity [6]. These limitations are currently the cause of prolonged therapies based on CPT-11 and prompted the combination of CPT-11 with other drugs to reach acceptable clinical results. One strategy to improve the vehiculation in water and enhance the therapeutic efficacy of SN38 is to use carriers and prodrugs [7,8]. Various systems have been successfully developed for this purpose, which include liposomes [9], inhibitor-drug complexes [10], antibody-drug complexes [11], protein-drug complexes [12], multi-component drug delivery systems [13], drug-loaded polymeric nanoparticles [14,15], graphene-based materials [13,16,17], to name a few.

Carbon dots (CDs), the latest member of the carbon nanomaterial family, are quasi-spherical carbon nanoparticles defined by a size <10 nm, a carbon core, and a surface rich in functional groups, such as carboxylic acid or amines, that is responsible for their hydrophilic properties [18,19]. Besides the water solubility, the most peculiar property of CDs is their fluorescence (FL) that prompted their fast rise for bioimaging and therapeutic applications [20,21]. In preparing drug-delivery systems, also their tunable and functionalizable surface after their synthesis, usually without the need of postsynthetic modification, combined with their low toxicity and easiness of biological clearing and degradation by the excretory system, have provided an advantage over other (carbon) nanomaterials [22–26]. All these properties make CDs an appealing nanomaterial for developing multifunctional drug-carrier systems that allow improved solubility of hydrophobic drugs, and localization analysis by exploiting CDs as bioimaging agents [27]. However, the possible beneficial effects of a CD-SN38 hybrid material have not been investigated so far.

Here, we report the design and preparation of a covalent CD-SN38 hybrid material via an acid-cleavable carbamate linkage. The hybrid material retains the fluorescence emission and the water solubility of the CDs, thus offering opportunities for both bioimaging and drug delivery. We demonstrate that the slow drug release promotes prolonged drug efficacy, thereby pointing at advantages for future *in vivo* biological systems that include minimizing the loss of the drug in circulation and general systemic toxicity and, additionally, maximizing the release of the drug in the nucleus in order to affect the DNA replication [28]. The hybrid material CD-SN38 is evaluated for cancer treatment on an *in vitro* model using enteric human colon cancer cells (HT29) through bioimaging localization and cytotoxicity studies [29,30]. The mechanism of the possible interference of the material on the CRC cell cycle is monitored by analyzing the expression of two key molecules: the cyclin-dependent kinase 7 (CDK7) and the antigen Ki-67 [31,32]. Also, given the importance of creating a cancer niche during cancer progression [33], we further evaluate the effects on the tumor microenvironment (TME) by examining the cell exposure to the hybrid material via analysis of the extracellular matrix (ECM) and its principal component collagen type I alpha 1 (COL1α1) and regulatory factor transforming growth factor-beta (TGFβ) [34–36]. Ultimately, this work demonstrates a covalent hybrid CD-SN38 system in which the slow and prolonged pH-sensitive release of the drug results in a cell cycle, cytoskeleton and niche CRC toxicity where the CDs can be used as bioimaging agent.

2. Materials and methods

Ultrapure water was obtained by a MilliQ™ water purification system (water resistivity of 18.2 MΩ at 25 °C). All the solvent and reagents (reagent grade) were bought from Sigma-Aldrich and used without further purification. Size exclusion chromatography (SEC) was carried out using Sephadex™ LH-20 as stationary phase and methanol as mobile phase. Transmission electron microscopy (TEM) was performed on a JEOL JEM-1400PLUS transmission electron microscope operating at an acceleration voltage of 120 kV from drop cast of aqueous samples (concentration of few mg mL^{-1}) on a carbon-coated 300 mesh copper grid. TEM images were analyzed using Gatan Microscopy Suite as TEM-image analysis software. Atomic force microscopy (AFM) was performed on a Nanoscope IIIa VEECO Instruments microscope from drop cast of aqueous samples (concentration of few mg mL^{-1}) on a mica substrate. AFM images were examined using Gwyddion 2.50 software. Dynamic light scattering and Z-potential measurements were performed on a Malvern DLS Litesizer 500 from aqueous samples. Fourier-transform infrared spectra (KBr) were recorded on a Perkin Elmer 2000 spectrometer. ^{1}H NMR spectra were obtained in DMSO-d_6 on a Varian Inova spectrometer (500 MHz) using the solvent residual peak as the internal reference. Self-diffusion coefficient evaluations were carried out using a Varian Inova (500 MHz) NMR spectrometer equipped with Performa II-Z gradient coils (Varian, Palo Alto, CA, USA) using a diffusion gradient length of 3.0 ms and a diffusion delay of 75.0 ms. UV–Vis spectra were recorded on an Agilent Cary 5000 UV–vis spectrophotometer, using quartz cells with a path length of 1.0 cm. Fluorescence emission spectra were recorded on an Agilent Cary Eclipse fluorescence spectrophotometer, using quartz cells with a path length of 1.0 cm. Fluorescence quantum yield (QY) measurements were performed exploiting the relative determination using quinine sulfate or fluorescein as standard. SN38 release studies were performed using dialysis (molecular weight cutoff 0.5-1 KDa) from 1.5 mL of a 570 μg mL^{-1} CD-SN38 solution (PBS at pH 7.4 or MilliQ water adjusted at pH 5.3 with HCl) against 14 mL of dialysate, at 37 °C and under slow stirring; 1 mL of the dialysate was withdrawn at different time intervals (and replaced with an equal volume of fresh solution at pH 7.4 or pH 5.3), dried under reduced pressure and freeze-dried overnight, redissolved in DMSO, filtered through a 45 μm PTFE filter and analyzed by HPLC (Agilent 1260 Infinity II, 15 min via gradient 95–5 → 5–95 of H_2O (+0.1% HCOOH)–MeCN, detection by UV–Vis absorption at 390 nm). The same HPLC parameters were applied for the standard calibration curve determination reported in Figure S1. Human Colorectal Adenocarcinoma Cell Line HT29 (ATCC® HTB-38™) was acquired by ATCC (ATCC, LGC Standards S.r.l, Milan, Italy).

2.1. In vitro studies

The studies were performed on HT29 cells, conditionally immortalized human podocytes (HciPodo, from University of Bristol, Bristol, UK), and glomerular endothelial cells (HciGEnC, from University of Bristol, Bristol, UK) as controls (Cell Culture and Cytotoxicity Assay). The cells were exposed to CDs or CD-SN38 or SN38 for 24, 48, and 72 h. IF and qRT-PCR analyses were used to explore respectively the CDs cell distribution and the impact of the different experimental exposures on cell cycle and tumor microenvironment (cell morphology, nanoparticles uptake, immunocytochemistry and qRT-PCR analysis).

2.2. Synthetic procedures

CDs were synthesized according to our previously reported procedure [37]. Typically, a solution of L-arginine (L-Arg, 40.0 mg, 230 μmol),

8-(4-carboxyphenyl)-1,3,5,7-tetramethyl-boron-dipyrromethene (BODIPY, 22.0 mg, 59.8 μmol) and ethylenediamine (EDA, 8 μL, 115 μmol) in MilliQ water (70 μL) was heated by microwave at 200 °C, 5 psi, 200 W for 180 s. The reaction mixture was then diluted with few milliliters of water, filtered through a 0.1 μm microporous membrane. The solution at pH 7.2 was filtered once again through a 0.1 μm microporous membrane, dialyzed in the dark against pure water through a dialysis membrane (molecular weight cutoff 0.5-1 KDa) for 48 h, and lyophilized obtaining a red solid (Kaiser Test 900 $\mu mol_{NH2}\ g^{-1}$), which is stored in a desiccator in the dark until characterization or use. CD-SN38 was prepared adapting a reported protocol [38]. SN38 (5.91 mg, 15.06 μmol), *p*-nitrophenyl chloroformate (5.65 mg, 28.03 μmol), and DIEA (10 μL, 57.41 μmol) were dissolved in DMF (0.5 mL) and the resulting solution was left stirring at RT for 1 h. A solution of CDs (50 mg, 45.00 μmol) in a mixture of DMF (7.5 mL) and MeOH (2.5 mL) was added to the previous one and the whole mixture was stirred at RT for 24 h. The Kaiser test was used to track the progress of the reaction. The reaction was then dried under vacuum, the brownish residue was dissolved in MeOH (1.5 mL) and purified by size exclusion chromatography using MeOH as mobile phase. The methanolic fractions were collected and dried under vacuum. Finally, the residue was dissolved in water and freeze-dried obtaining a fine reddish powder (52.93 mg; Kaiser Test 100 $\mu mol_{NH2}\ g^{-1}$).

2.3. Cell culture

According to manufacturer's instructions, HT29 cells were cultured in McCoy's 5 A medium supplemented with 10% fetal bovine serum (FBS) and 100 U mL^{-1} penicillin, 100 μg mL^{-1} streptomycin in the incubator at 37 °C and 5% CO_2 and used after 3–5 days of seeding. The pH of the HT29 culture medium (T = 37 °C) was monitored at 24, 48 and 72 h (Table S1). Studies were conducted after 24, 48, and 72 h, with CDs, CD-SN38 or SN38 using a concentration below the LD50 value. The untreated cells samples (CTRL) are cells cultures treated only with the culture medium. In the case of Ki-67 IF, a cells synchronization by serum deprivation (only McCoy's 5 A medium and 100 U mL^{-1} penicillin, 100 μg mL^{-1}) for 24 h was applied. Control cell lines HciPodo and HciGEnC were used to confirm the absence of CDs cytotoxicity.

2.4. Cytotoxicity Assay

To determine cell viability, HT29 cells were plated at a density of 10 000 cells $well^{-1}$ in 96 well plates at 37 °C in 5% CO_2. The cells were then incubated with a dosage of CDs from 0.003 to 1 mg mL^{-1}, SN38 from 0.5 to 100 μM, and CD-SN38 from 0.43 to 140 μM for 24, 48, and 72 h (the dosage of CD-SN38 is referred to the SN38 μM). For cell viability assessment, we used MTT solution (3-[4,5-dimethylthiazol-2-yl]-2,5-diphenyltetrazolium bromide, Thermofisher). The MTT is reduced by NAD(P)H-dependent enzymes in formazan crystals which can be assessed by spectrophotometer. At each time point, 10 μL of MTT was added to each well for 4 h, equaling one-tenth of the original volume of the wells. The medium was then removed, and formazan crystals were solubilized with acid isopropanol (0.04 N HCl in absolute isopropanol) for 2 h at 37 °C in a humidified chamber. The absorbance at 570 nm for each well was then determined by a spectrophotometer (SAFAS Flx-Xenius Monaco). The blank was calibrated at 570 nm, using a culture medium without cells. Background at 650 nm was subtracted to each reading and the obtained average values were subtracted with the average value of the blank. The results were expressed as % of cell death and were related to the control wells containing only the cell culture medium. The percentages were calculated by comparing the results to the average absorbance of the controls samples at time=0. Podocytes and endothelial cells were plated at a density of 25 000 cells $well^{-1}$ in 96 well plates at 37 °C in 5% CO_2 with an increasing dose of CDs from 10 to 200 μg mL^{-1} for 24, 48, and 72 h following the same procedure adopted for HT29, as previously described.

2.5. Cell morphology, uptake, and immunocytochemistry

For the immunocytochemistry study, the cells were seeded at a density of 40 000 cells $well^{-1}$ in 12 well plates on coverslips and treated with 0.1 mg mL^{-1} of CDs, 1 μM of SN38, and 0.1 mg mL^{-1} CD-SN38 (containing 14 μM SN38) for 24, 48 and 72 h. The cells were monitored daily to assess morphology and confluence in the control condition and after incubation by Axiovert 25 inverted microscopy (Carl Zeiss SpA, Arese, Milano, Italy). At each time point, the cells were fixed in 4% paraformaldehyde for 10 min at RT or in cold acetone/methanol (ratio 1:1) for 30 min, depending on the primary antibody. The fixation was performed with 4% paraformaldehyde for 10 s for the visualization of CDs. For Ki-67 and Collagen Type I analysis, after fixation the cells were then permeabilized with 0.3% of Triton (TX−100, Sigma Aldrich) in PBS for 30 min at RT, and then incubated with 1% of BSA blocking solution in PBS for 1 h at RT. A direct IF of actin filaments was performed to assess cytoskeleton integrity, adding 50 μg mL^{-1} of Tritc-labelled F-actin (Sigma-Aldrich) in PBS for 30 min. For ECM1 analysis, the cells were incubated with 1 mg mL^{-1} Collagen Type I-FITC conjugate (Sigma-Aldrich) for 1 h at RT. For indirect IF analysis, 2.5 μg mL^{-1} rabbit anti-Ki-67 (Abcam, Milan, Italy), 5 μg mL^{-1} as primary antibody in PBS were used and incubated o. n. at 4 °C. Samples were then washed with PBS and fluorescent secondary antibodies were applied for 1 h at RT: Alexa Fluor 546 goat anti-rabbit IgG for Ki-67 (Invitrogen, Milan, Italy). The nuclei were stained with DAPI for 1 h at RT. The specificity of Ab labeling was demonstrated by the lack of staining after substituting the primary antibody with rabbit immunoglobulins (Invitrogen, Milan, Italy). Slides were mounted with Fluorsave aqueous mounting medium (Calbiochem, Merck CheSN-NPls Ltd, Nottingham, UK). Tritc-labelled F-actin was used to visualize actin filaments using filter 43 HE (excitation BP 550/25 beam splitter FT 570; emission BP 605/70), λ_{exc} = 545 nm, λ_{em} = 573 nm, and exposure time = 372 ms; FITC conjugate Collagen Type I was used to visualize the collagen using filter 38 HE (excitation BP 470/40 beam splitter FT 495; emission BP 525/50), λ_{exc} = 490 nm, λ_{em} = 520 nm and exposure time = 610 ms; Alexa Fluor 546 was used to visualize Ki-67 using filter 43 HE (excitation BP 550/25 beam splitter FT 570; emission BP 605/70), λ_{exc} = 556 nm and λ_{em} = 573 nm and exposure time = 372 ms; the nuclei stained with DAPI were visualized using filter 34 (excitation BP 390/22 beam splitter FT 420; emission BP 460/50), λ_{exc} = 364 nm, λ_{em} = 454 nm and exposure time = 39 ms; the nanoparticles were visualized using filter 38 HE (excitation BP 470/40 beam splitter FT 495; emission BP 525/50), λ_{exc} = 495 nm and λ_{em} = 507 nm and exposure time = 610 ms. Control experiments where the nanoparticles were visualized with the experimental setup used to visualize the cell staining dyes show that our experimental conditions provide negligible overlap of the signals; no signal from the nanoparticles can be detected after the acetone cells fixation used for collagen staining. The characteristic filter HE (high efficiency) of ZEISS compared to a standard filter are distinguished by steep cut-off edges and extremely high transmittances. Cell microscopy images were acquired by Zeiss AxioObserver microscope equipped with a high-resolution AxioCamMRc5 digital videocamera and Apotome system based on a statistical complex algorithm to obtain a recovery of the missing element and a reduction of the interference and a high quality of the structures examined. Some images were acquired with the 3-D Z-Stack system (1 μM/section). The images are recorded by AxioVision software 4.8 (Carl Zeiss). The IMAGE J program was used for the COLIαI quantification.

2.6. Lysosomes and co-localization studies

For the localization of CDs in the subcellular compartments, and in particular in the lysosomes, the cells were counterstained with LysoTracker Red DND 99 (Thermofisher) after the addition of 0.1 mg mL^{-1} of CDs or CD-SN38 (0.1 mg mL^{-1}) for 12, 24 and 48 h. Next, the medium was changed with pre-warmed probe-containing medium at a final concentration of 50 nM and then incubated for 1 h at 37 °C 5% CO_2. After

incubation the cells were fixed with formalin for 10 s and the slides were mounted and visualized by fluorescence microscope as reported in section 2.5. The fluorescence microscope settings are: DND99-labelled λ_{exc} = 577 nm, λ_{em} = 590 nm, and exposure time = 372 ms; 495 and 507 nm were used as excitation wavelengths for the nanomaterials with an exposure time = 610 ms.

2.7. qRT-PCR analysis

Cells were seeded at the confluence of 40 000 cells well^{-1} in triplicates and treated with 0.1 mg mL^{-1} of CDs, 1 μM of SN38, and 0.1 mg mL^{-1} CD-SN38 (containing 14 μM SN38), for 24, 48, and 72 h. Total RNA of HT29 was extracted at each condition by Trizol (Invitrogen) and precipitated by chloroform-isopropyl alcohol, washed in ethanol 75%, resuspended in nuclease free-water, and quantified by spectrophotometry after treatment with DNase. The cDNA was then prepared from 1 μg of RNA using the iScript Select cDNA Synthesis Kit and oligo (dt)20 primers (Bio-Rad, Milan, Italy). The mRNA extracted was used to evaluate CDK7, proliferation marker protein Ki-67, COL1α1, ECM1, TGFβ1, CASP3 and TLR4. Data were normalized against the expression of housekeeping gene Ribosomal Protein L4 (RPL4) (Primer list in Table S2). To verify the absence of genomic DNA in the samples qRT-PCR was performed in triplicates also on the original RNA (minus-reverse transcriptase). Real-Time qRT-PCR analyses were run with iQ Sybr Green Supermix (Bio-Rad) on a MyIQ instrument (Bio-Rad), and data were analyzed by the IQ5 Bio-Rad Software.

2.8. Statistical analysis

Experiments were conducted on at least 3 replicates for each condition and time point. Data were expressed as mean ± standard deviation (SD), Student's t-test was applied to determine significance ($p < 0.05$). For qRT-PCR analysis, relative RNA abundance was determined using the comparative Ct method. The fold-change (FC) calculated by the software, was evaluated according to the following formula:

$$\sigma_{FC} = FC \ln 2 \sqrt{\left(\sigma_x \frac{2}{n_x} + \sigma_y \frac{2}{n_y}\right)}$$

The fold change error bars represent the standard deviation (σ) of the fold change (FC). p values were calculated based on Student's t-test of the replicate 2 (−Delta Ct) values for each gene in the control group and treatment groups, and p values < 0.05 were considered significant. Symbols "*" indicate significant differences: "*" = $p < 0.05$, "**" = $p < 0.01$, "***" = $p < 0.001$.

3. Results and discussion

3.1. Synthesis and characterization

The synthesis of CDs via bottom-up approaches provides straightforward procedures and the possibility to tailor core and surface properties via the choice of molecular precursors [39]. Our group reported the use of arginine and ethylenediamine for the microwave-assisted synthesis of nitrogen-doped CDs with a surface rich in various functional groups, such as amino groups that can be exploited for covalent functionalization [40,41]. More recently, we demonstrated that the introduction of a boron-dipyrromethene (BODIPY) dye in the precursor's mixture afforded small (~ 2.0 nm) and water-soluble BODIPY-doped CDs with good photostability, and blue and green FL emission by retaining the emission features of both the carbon nanoparticle and the dye [37]. While there have been notable reports on tuning the FL emission properties by modulating synthetic conditions such as the reaction temperature, the demonstration of dye-doped CDs by us and others provide a rational approach towards CDs with multicolored emission [27,42], which is of particular value to afford CDs with tailored properties for bioimaging applications. Here, we settled on our recent synthetic procedure for preparing BODIPY-doped CDs (CDs from now on) with a surface rich in amino groups (Fig. 1).

For the conjugation reaction, SN38 was firstly activated by reacting the phenolic hydroxyl at position 10 with *p*-nitrophenylchloroformate, forming a reactive carbonate group (Figure S2) [38]. The activated SN38 was then reacted with primary amino groups presents on the surface of CDs to form a carbamate bond (Fig. 1). The hybrid material, named CD-SN38, was purified by size exclusion chromatography, using methanol as the mobile phase, and was finally obtained as a light-red powder after the removal of the solvent under vacuum and further freeze-drying from water. Atomic force microscopy and transmission electron microscopy showed an increased size for CD-SN38 of around 5 nm compared to the value of around 2 nm for CDs (Figures S3-S4). The increase in size of the hybrid material was further probed by dynamic light scattering measurements (Figure S5). The change in zeta potential value from −11.93 ± 2.40 mV for CDs to −16.20 ± 0.06 mV for CD-SN38 is consistent with the decreases of protonated amine sites in the hybrid material. The FT-IR spectrum of CD-SN38 showed bands analogous to those of SN38 and CDs at around 1700-800 cm^{-1} (Fig. 2a and Figure S6). Compared with CDs, the hybrid exhibited additional shoulder peaks at 1400 cm^{-1} and 1590 cm^{-1} attributed to the C–N stretching band and N–H bending vibration of the amide linkage, and a peak at around 3200 cm^{-1} ascribed to the N–H stretching vibration of the amides. The formation of the covalent hybrid material was probed also by ^{1}H NMR spectroscopy. The ^{1}H NMR spectrum of the hybrid shows the typical signatures of both CDs and SN38, and the disappearance of the phenolic proton in position 10 (singlet at 10.30 ppm) of the SN38 structure supports the formation of the carbamate bond (Fig. 2b and Figure S7). Proton signals of the hybrid can experience broadening because of the slower molecular motion of the drug [43]. In addition, diffusion-ordered spectroscopy NMR of the hybrid showed a homogeneous diffusion of the peaks assigned to SN38 and CDs indicating the presence of a single species in solution and, therefore, supporting the successful formation of the covalent hybrid (Figure S8).

The optical properties of the hybrid were studied by UV–Vis and FL emission spectroscopies (Fig. 2c). The UV–Vis spectrum of CD-SN38 showed the typical signatures of both SN38 (π→π* transitions at 370 and 388 nm) and CDs (at 501 nm) (Fig. 2c, black traces, and Figures S9-13) [37,44]. Fluorescence spectroscopy revealed a dual emission of the hybrid material upon excitation at 334 and 500 nm (Fig. 2c, red traces, and Figures S9-13). Furthermore, UV–Vis and FL spectra of the hybrid in water demonstrated the enhanced water solubility of the drug once attached to CDs. The loading content of SN38 in the hybrid material was calculated as 140 nmol mg^{-1} via a standard calibration curve method (Figure S14).

Since different pH values are found in different cell compartments, a possible pH-dependent drug release of CD-SN38 was investigated at 37 °C at pH 7.4 and pH 5.3. The amount of released SN38 was measured by HPLC at time intervals over a period of 100 h (Fig. 2d and Figure S15). The initial rapid release is followed by a slow and steady release of SN38 at both pH values, reaching 80% or 50% after 24 h of incubation at pH 5.3 or pH 7.4, respectively. The *N*-monosubstituted carbamate of phenol is labile toward hydrolysis and the rate of release is higher at the lower pH value because the carbamate linkage is prone to faster hydrolysis in acidic conditions [28,45]. After internalization, the release of SN38 from the hybrid material would therefore increase in the acidic compartment of the nucleus affecting the DNA replication. Around 95% of drug is rapidly released from the dialysis bag containing free SN38 within 5 h at both pH 5.3 and 7.4 indicating a release controlled by diffusion, which is significantly faster than the release observed from the hybrid material (Figure S16). These results point at the advantage of the hybrid material in controlling the drug release and prolonging its cytotoxic effect, which imply the possibility of avoiding multiple administrations while maintaining its effectiveness.

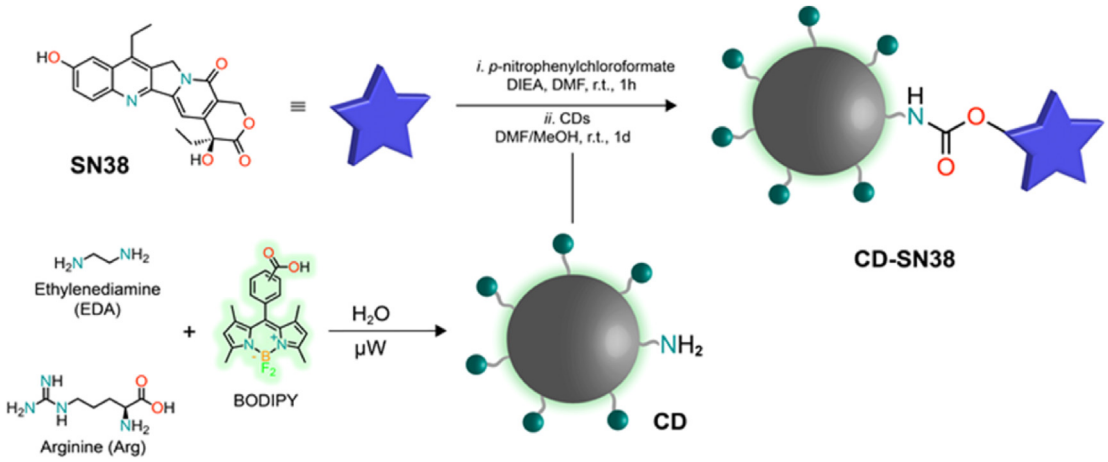

Fig. 1. Synthetic scheme for the covalent hybrid CD-SN38 used in this study.

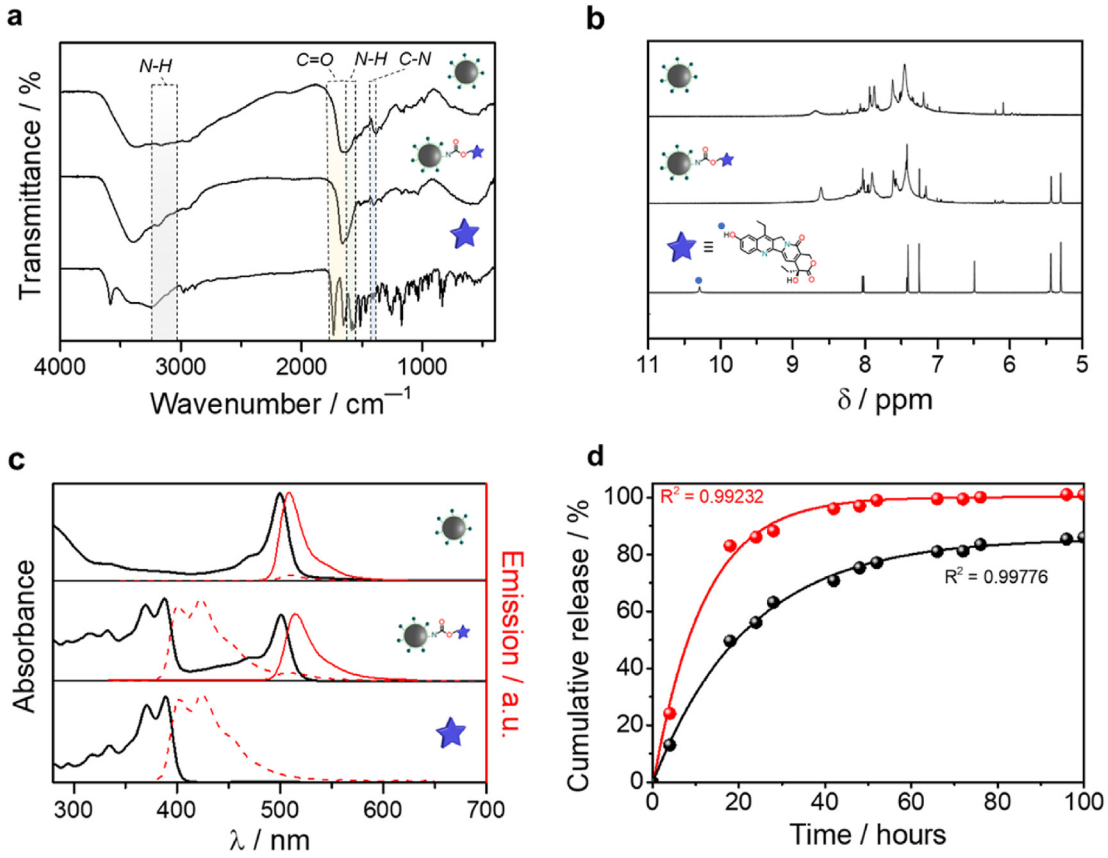

Fig. 2. (a) FT-IR (KBr) and (b) ^{1}H NMR (DMSO-d_6, 298 K, 500 MHz) spectra of CDs (top), CD-SN38 (middle), SN38 (bottom). (c) UV–Vis (black solid line), and FL (red dotted line for excitation at 334 nm, red solid line for excitation at 500 nm) spectra of CDs (top), CD-SN38 (middle) and SN38 (bottom) (DMF, 298 K). (d) Quantitative analysis of the SN38 release from CD-SN38 at 37 °C and incubated at pH 7.4 (black trace) or pH 5.3 (red trace); the curves indicate the fit to experimental data using a first-order release model.

3.2. Cell viability and localization studies

The *in vitro* analysis of CD-SN38 was firstly approached by cytotoxicity studies to confirm its feasibility as drug-carrier and establishing the experimental concentrations (Figure S17).

The applicability of our CDs as drug carriers was investigated by an MTT assay based on succinate dehydrogenase reflecting the mitochondria metabolic activity towards non-tumoral and more susceptible endothelial (HciGEnC) and podocytes cells (HciPodo) (Figure S18) [46]. In these cases, we observed a maintained low toxicity (cells death <25%) in the explored concentration range (10–200 μg mL^{-1}). In a similar fashion, the MTT assays of CDs applied to HT29 showed good biocompatibility and allowed the selection of an experimental concentration of 0.1 mg mL^{-1} for CDs, 1 μM for SN38 and 0.1 mg mL^{-1} CD-SN38 (containing 14 μM SN38), which was made considering the higher value recorded under the LD50 after exposure time of 48 h, e.g. 13 ± 3.9% for CDs, 43 ± 4.7% for SN38 and 43 ± 5.9% for the CD-SN38 hybrid (Figure S17). CDs exhibited concentration-dependent cytotoxicity for

tumoral HT29 cells, which was, however, significantly lower than the LD50 value obtained at concentrations up to 1 mg mL^{-1} and exposure times up to 72 h. These results indicate the low cytotoxicity of our CDs, which is in accordance with previous reports [27,47], and therefore support their use as a safe drug carrier. Both SN38 and CD-SN38 exhibited, as expected, a concentration-dependent cell death, with a trend indicating more pronounced cytotoxicity for the former than for the latter (Figure S17). The presence of the CDs at similar SN38 dosages mitigates the toxicity of the drug because the higher concentration below the LD50 threshold was 1 μM SN38 and 0.1 mg mL^{-1} (containing 14 μM SN38) CD-SN38 (Figure S17). Despite a pronounced difference in the concentration between SN38 and CD-SN38, we observe that the higher drug effect was recorded at 48 h of exposure for both systems, but it was maintained constant up to 72 h in the case of CD-SN38 (cell death of 43% and 41% at 48 and 72 h, respectively) (Figure S17c). Compared to the hybrid material, the cytotoxicity of free SN38 started to decrease faster after 48 h (cell death of 43% and 26% at 48 and 72 h, respectively) (Figure S17b). These last observations suggest that the apparent lower toxicity of the SN38 when conjugated to CDs could be explained by the slower and possibly persisting drug release that might prolong the pharmacological activity, which agrees with the drug release study (Fig. 2d).

We performed cell uptake studies via FL bioimaging during the cytotoxic action after 30 min, 60 min, 120 min, 12 h, and 24 h of incubation recording images with 3-D Z-Stack (Fig. 3a) in order to assess if CDs, bypassing the three-dimensional scaffold embedded in the TME, are able to reach the cytoplasm and then the nucleus of HT29. CDs and CD-SN38 were localized by FL contrast imaging (green), the nuclei were labelled with 4′,6-diamidino-2-phenylindole (DAPI, blue) and the cytoplasm with the actin filaments with tetramethyl rhodamine (TRITC, red). The cell uptake resulted very rapid starting from 30 min for both CDs and CD-SN38. The capacity of CDs to reach the cytoplasm and the nucleus of HT29 cells is an important clue to understand if the nanomaterial could be considered as active sources of interferences for the natural intracellular activities. For this reason, we further studied the time of the CDs efflux and/or degradation. The nuclear and cytoplasmic uptake and distribution of CDs, SN38, and CD-SN38 were then examinate after 24, 48, and 72 h of incubation (Fig. 3b). For both CD-SN38 and CDs, the cytoplasmic and nuclear uptake were visible at 24 h and nearly vanished at 48 h and 72 h. These results clearly demonstrated that there is no accumulation of the CDs in the cells because of their good clearance, which is a desirable property for a successful drug-carrier material. The influence of CDs, SN38, and CD-SN38 on the actin filament, an essential part of the cytoskeleton deputed to crucial cell roles (e.g., structural support, mitosis, organelles transport, communication), was also examined (Fig. 3b). The well-organized actin filament is clearly visible in the control sample (CTRL) and was maintained after exposure to CDs up to 72 h, but the treatment with both SN38 and CD-SN38 caused disorganization and a strong accumulation of the actin filaments around the nuclei at all the time points examinated. These results highlight that the SN38 efficacy is maintained when it is administered as CD-based hybrid material. Moreover, to investigate the possible CDs metabolization mechanism we evaluated the lysosomes internalization of CDs with a lysotracker label experiment at 12, 24 and 48 h (Fig. 3c). CDs and CD-SN38 were localized by FL contrast imaging (green), the nuclei were labelled with DAPI (blue) and the lysosomes with TRITC (red). The lysosome-CDs co-localization can be observed after 12 h of incubation indicating the beginning of a metabolic digestion pathway, and it almost disappeared at 48 h confirming the absence of toxic accumulation.

The effects of CDs, SN38, and CD-SN38 on the HT29 cell proliferation were further analyzed by both optical microscopy and the measurement of cells metabolic activities at 24, 48, and 72 h (Fig. 4). Untreated HT29 cells progressively grew (Fig. 4a–d, 4s), but the CD treatment resulted in an initially stopped (Fig. 4e–h, 4s) and thereafter decreased cell proliferation (Fig. 4s), without any major modification of cell morphology and with an apparent concomitant increase of ECM, considered the main component of cancer niche (Fig. 4h). This result further confirmed a non-toxic effect of CDs, indeed the cells conveyed the energy on producing a natural and self-protecting matrix (cancer niche) instead of devolving the energy in the proliferation [36,48]. A significant difference between CDs and CD-SN38 confirmed the non-toxicity of the CDs compared to CD-SN38 and it was observed at all the time points analyzed (24 h $p = 0.0003$, 48 h $p = 0.0005$, 72 h $p < 0.0001$). The treatment with either CD-SN38 or SN38 induced a marked and progressive decrease of cell proliferation, production of debris, and destruction of the HT29 structure. It is important to highlight that, while no difference was observed at 24 and 48 h between CD-SN38 and SN38 (24 h $p = 0.13$, 48 h $p = 0.26$), at 72 h the significance ($p = 0.0013$) indicated more prolonged SN38 effect on cell proliferation when the drug is conjugated with CDs. More importantly, the cells showed an apparent trend of recovery after 72 h only in the case of SN38, providing another piece of evidence of a slower release and, possibly, a persisting effect of the drug when loaded on CDs (Fig. 4i–n, 4o-r, 4s).

3.3. Cell cycle monitoring

Encouraged by the cytotoxic effect of the CD-SN38 hybrid material, the mechanism of cytotoxicity was investigated via the analysis of the cell cycle. The study involved probing, via quantitative reverse transcription polymerase chain reaction (qRT-PCR), of the encoding genes of two typical proteins, CDK7 and Ki-67, which are expressed in the different phases of cellular reproduction.

CDK7, a component of the Ckd-activating kinase family, is an important target for the treatment of several cancers [49]. CDK7 is an essential component of the transcription factor TFIIH, which is involved in the transcription initiation by controlling the DNA repair and the activity of enzymes involved in the regulation of cell cycle progression (such as cyclin-dependent kinases 1, 2, 4, and 6) [50]. While no changes in the expression of CDK7 were observed during natural HT29 growth, SN38 induced a marked reduced expression after 24 h ($p = 0.002$) and 48 h ($p = 0.009$), with a trend to rebound after 72 h ($p = 0.54$) (Figure S19). The treatment with CDs induced an increase of the CDK7 levels ($p = 0.01$ at 24 h, and $p = 0.007$ at 48 h) with a strong up-regulation after 72 h ($p < 0.001$), but these stimulatory effects on CDK7 were completely abolished when CDs were loaded with SN38 with the most evident effect of the drug being visible at 48 h ($p = 0.11$ at 24 h, $p = <0.001$ at 48 h, $p = 0.8$ at 72 h) (Figure S19). However, the drug exhibited a more prolonged effect when it was administered in the form of the hybrid as opposed to when it was in the free form (Figure S19). The strong up-regulation observed after the CD treatment could be interpreted in two different ways. The first, positively, by attributing the upregulation to the transcription role of CDK7, probably dedicated to the production of matrix proteins observed in the optical images (Fig. 4h) that confirms the non-toxicity of the treatment. In the second case, negatively, the treatment with CDs could increase the possibility of HT29 proliferation after 72 h. However, even in the latter case, the effect is completely abolished when the CDs transports the drug. These results further pointed at the sustained effects of the drug for the hybrid material, but the pleiotropic activities of CDK7 made the interpretation of the cytotoxic mechanism difficult. Previous literature reports that a highly selective inhibitor BS-181 of CDK7 significantly impeded the development of collagen-induced arthritis in mice, supporting therefore the existence of a correlation between the overexpression of CDK7 and the matrix (COLIαI) production [51]. For example, a study on scleroderma fibroblast reports that Roscovitine inhibition of the transcriptional CDKs (CDK7 and CDK9) impacts gene expression inhibiting the COLIαI expression [52].

The analysis of the sensible-oncologic prognostic proliferation marker Ki-67 was carried out to gain more insights into the possible effects of the treatments on proliferative kinetics. The investigation was supported by apotome fluorescence microscopy via the staining of the protein (Alexa Fluor 546) and the analysis of the mitosis phase after 48 h (Fig. 5). The

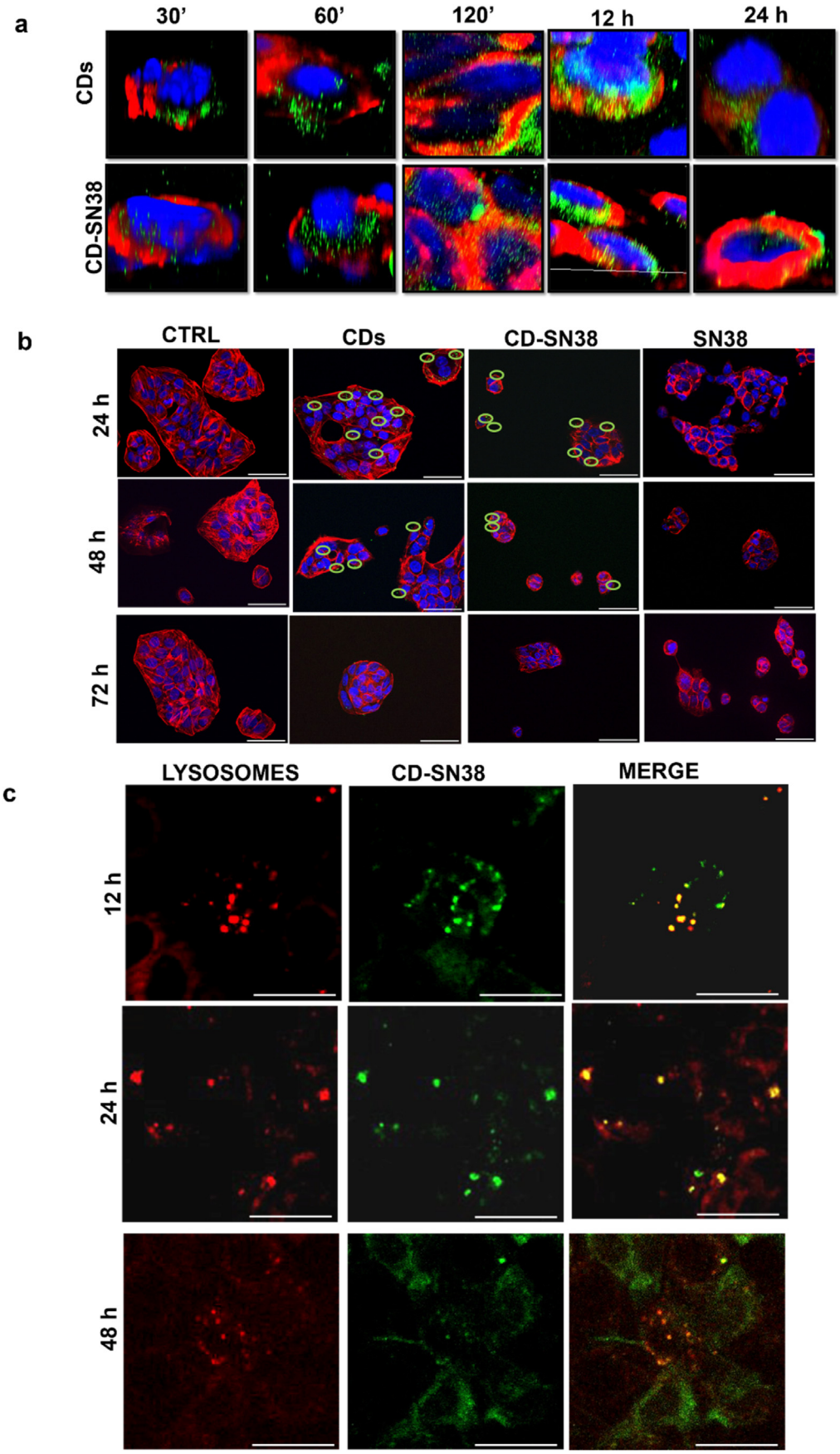

Fig. 3. (a) HT29 nucleus (blue) and actin filament (red) imaging after 30 min, 60 min, 120 min, 12 h, 24 h of incubation with 0.1 mg mL^{-1} of CDs (green) or 0.1 mg mL^{-1} of CD-SN38 (green). (b) HT29 nucleus (blue) and actin filament (red) imaging after 24 h, 48 h, 72 h of incubation with 0.1 mg mL^{-1} of CDs (green), 1 μM of SN38 and 0.1 mg mL^{-1} of CD-SN38 (green). (c) CD-SN38 (0.1 mg mL^{-1}, green) and lysosomes (red) co-localization IF in HT29 after 12 h, 24 h, 48 h of incubation. Scale bar: 50 μm.

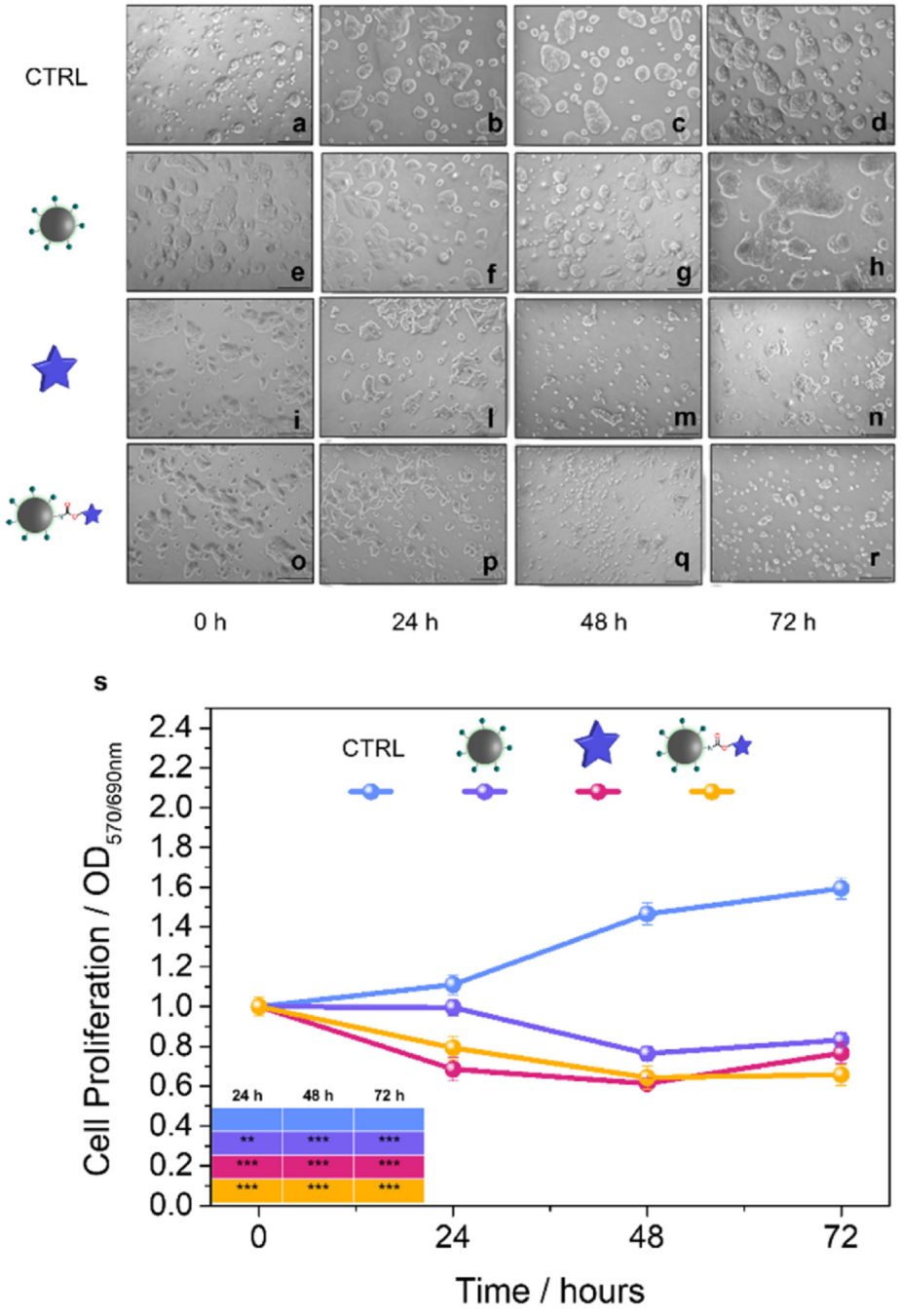

Fig. 4. HT29 microscopic optical images after 0 h, 24 h, 48 h and 72 h without (a–d) and with addition of CDs (e–h), SN38 (i–n) or CD-SN38 (o–r). Scale bar: 100 μm. Cell proliferation at the same conditions (s); n = 6/group. "*" indicates the significant difference versus HT29 reference sample (CTRL) after 24, 48 and 72 h "**" = $p < 0.01$, "***" = $p < 0.001$".

antigen Ki-67 is a specific marker of cell proliferation, which increases during the cell cycle (except G0, resting state) and it is principally associated with the mitotic phase, thereby allowing the correct separation of chromosomes [53,54]. During the natural growth, HT29 cells showed a scalar increase of Ki-67 (Figure S20a) following each step of the chromosomes division (Fig. 5a1-a5). Therefore, during the prophase, Ki-67 is well condensed in the center of the nucleus on the chromosome (Fig. 5a1). In the metaphase, Ki-67 was aligned with chromosome along the whole nuclear equator (Fig. 5a2). In the anaphase, telophase, and cytokinesis the Ki-67 followed the sister chromatids, which were separated from each other and pulled towards opposite ends in the cells (Fig. 5a3-a5).

The treatment with CDs resulted in a down-regulated expression of Ki-67 that is partially recovered after 48 and 72 h ($p = 0.004$ at 24 h, $p = 0.38$ at 48 h, $p = 0.86$ at 72 h) (Figure S20b), and in a multipolar chromosome spindle assembly checkpoint after 48 h during the anaphase (Fig. 5b3). Usually, the normal cell division is characterized by a bipolar mitotic spindle, with symmetrical segregation of chromosomes [53]. After CD addition, a rare mitotic aspect appeared, followed by a perfect recovery of the normal chromosome separation (Fig. 5b4-b5). This unusual, and yet unclear, phenomenon described in cancer cells [55,56], could be interpreted as a moment of stasis for checking the cell cycle, followed by a recovery of the normal mitosis, and confirmed once again the no-toxicity of CDs. The administration of SN38 induced a clear-cut

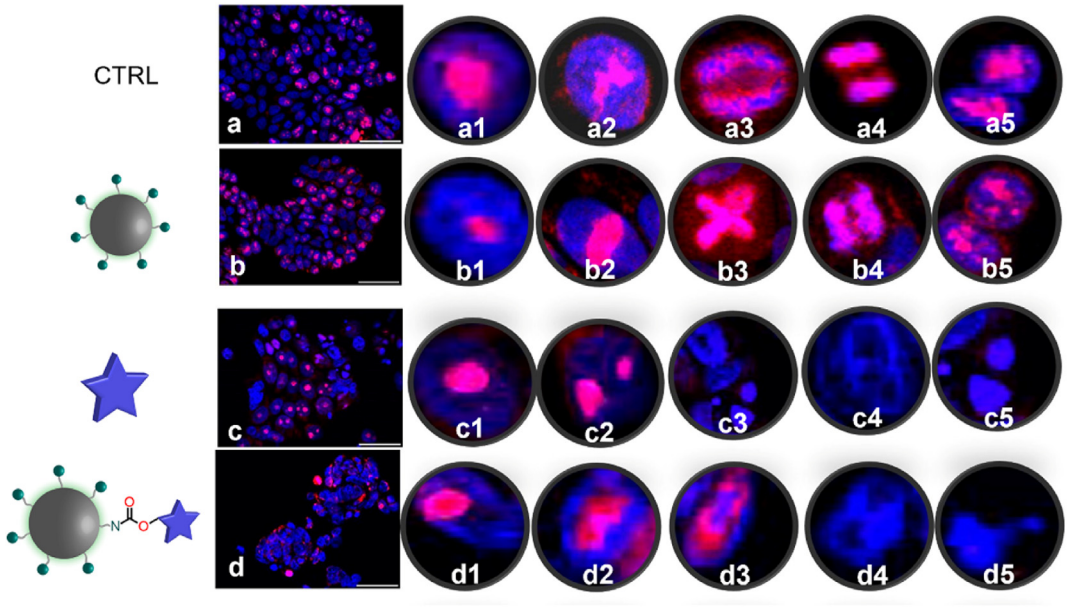

Fig. 5. Rhodamine immunofluorescence (IF) of Ki-67 (red) and nucleus (blue) in HT29 cells (a) and after 0.1 mg mL^{-1} CDs (b), 1 μM SN38 (c) or 0.1 mg mL^{-1} CD-SN38 (d) addition at 48 h. Scale bars: 50 μm. Representation of a panel of each mitosis phase after each treatment at each time point: Prophase (a1-d1), Metaphase (a2-d2), Anaphase (a3-d3), Telophase (a4-d4), Cytokinesis (a5-d5).

downregulation of Ki-67 that was visible after 24 h ($p < 0.0001$), followed by a recovery after 48 h ($p = 0.3$) and a strong rebound after 72 h ($p = 0.0008$) (Figure S20b). The rebound effect could be explained by the well-known release of debris from cells damaged by SN38, as shown also in our experiments (Fig. 4), which can stimulate cell growth [57]. Moreover, SN38 caused dysregulation of the chromosome distribution of Ki-67 already in the metaphase with subsequent complete disappearance of chromosomes in most cells (Fig. 5c2-c5).

The Ki-67 expression after CD-SN38 treatment mimicked the one observed after SN38 treatment for up to 48 h ($p < 0.0001$ at 24 h and at 48 h) (Figure S20b). However, the rebound effect at 72 h ($p = 0.12$) observed with SN38 was absent when CD-SN38 was administered. This last observation remarks another beneficial effect from the administration of SN38 conjugated to CDs because the absence of the rebound effect could be related to the deactivation of cell reproduction and then to a cytotoxic effect. Also, the chromosome dysregulation occurred later in the telophase in the case of CD-SN38 as compared with the free SN38 (Fig. 5d4-d5). These results support the hypothesis of a slower release of the drug from the hybrid material as the reason for a longer-lasting effect, which is consistent with the reduced toxicity upon the administration of the hybrid material as compared with the free drug. Given the Ki-67 behavior after the CDs addition (Figure S20), we believe that the observed up-regulation of CDK7 (Figure S19) is mostly directed to controlling matrix protein transcription and at a lesser extent to inducing cell proliferation. These results confirmed the great matrix production observed in the optical images (Fig. 4h).

Finally, we studied apoptosis and necrosis of HT29 cells by RT PCR 2 gene related to apoptosis caspase 3 (CASP3) and necrosis Toll-like receptor 4 (TRL4), respectively. CASP3 results indicated a significant apoptosis at 48 h only for SN38 and CD-SN38, and without significance between SN38 and CD-SN38 ($p = 0.2$ for CDs, $p = 0.008$ for CDs, $p = 0.001$ for CD-SN38) (Figure S21a). The TLR4 expression indicated no activation of necrosis at 48 h for none of the systems studies, i.e. CDs, SN38 or CD-SN38 (Figure S21b). These results are in agreement with a previous report showing the absence of necrosis in HT29 even after four days of incubation with SN38 [58,59].

3.4. Extracellular matrix analysis

We further evaluated the analysis of the extracellular matrix 1 (ECM1), considered one of the major TME components, interacting with a variety of extracellular and structural proteins (cell surface receptors, enzymes, and chemokines), to contribute to the maintenance of the TME itself [33,60]. As expected, no changes in the ECM1 gene expression were observed for the untreated HT29 cells between 24 and 72 h (Figure S22a). In contrast to the untreated cells, treatments with CDs, SN38, or CD-SN38 caused an increase of ECM1 till 72 h ($p = 0.0005$ for CDs, $p < 0.0001$ for SN38, $p = 0.0005$ for CD-SN38), which was faster and stronger in the case of SN38 (Figure S22c). The ECM dysregulation of its component could affect its stiffness and elasticity with a possible impact on CRC proliferation, migration, and metastasis [36]. The ECM1 study was therefore complemented by the analysis of COL1α1 expression, which is the major ECM component [60]. While a constant gene expression of COL1α1 was recorded during the natural cell growth (Figure S22b), treatment with CDs or SN38 produced the following two effects: (i) strong up-regulation after CDs addition only after 72 h ($p = 0.9$ at 24 h, $p = 0.001$ at 48 h, $p < 0.0001$ at 72 h); (ii) increased expression following SN38 treatment after 48 h followed by a decrease after 72 h ($p = 0.002$ at 24 h, $p < 0.0001$ at 48 h, $p < 0.0001$ at 72 h) (Figure S22d). We interpret these results based on the following rationale. Starting from the overexpression of COL1α1 after SN38 and CD-SN38 treatment at 48 h, the difference in the expression suggests a possible drug involvement in the mechanism, which is higher in the case of SN38 alone compared to CD-SN38 due to the slow release of SN38 from the hybrid material (Figure S22d). Regarding the COL1α1 overexpression after CD addition at 72 h, our results can be interpreted considering that a correlation exists between CDK7 and COL1α1, as described above (section 3.3) and reported in literature [51,52].

The increases in the CKD7 (Figure S19b) and COL1α1 (Figure S22d) expression following the CDs treatment might imply that the CDK7 production is mainly related to the COL1α1 protein production as a defensive mechanism and not to cell proliferation. To better understand the expression of COL1α1 during the studied time range, we probed the

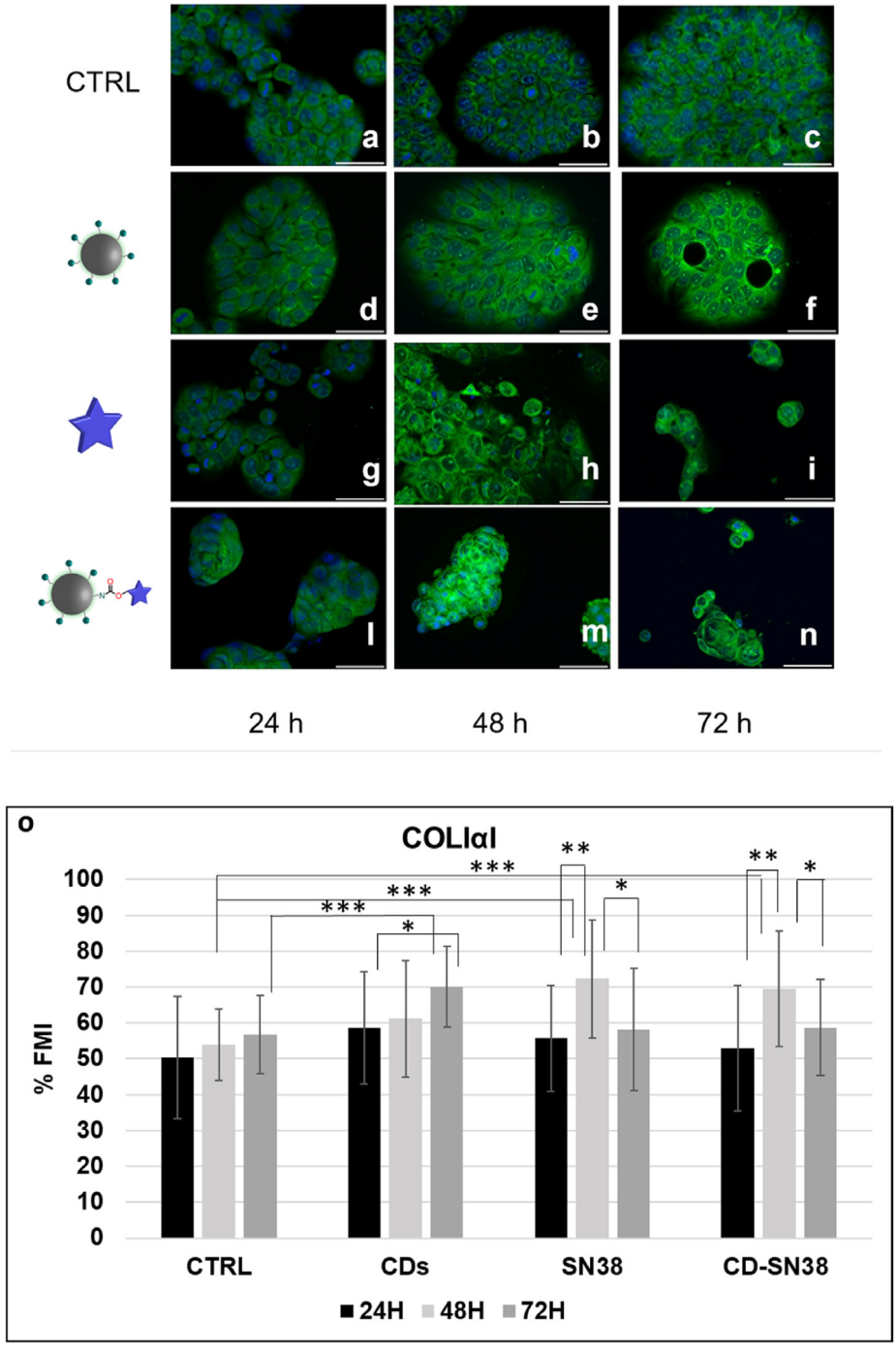

Fig. 6. Immunofluorescence (IF) of COLIαI (green) in HT29 (a–c) and after 0.1 mg mL^{-1} CDs (*d*–f), 1 μM SN38 (g–i) or 0.1 mg mL^{-1} CD-SN38 (l–n) addition at 24, 48 and 72 h of treatment (scale bars: 50 μm). (o) Quantification of COLIαI immunostaining. N = 19. * = $p < 0.05$, ** = $p < 0.01$, *** = $p < 0.001$.

protein (Fig. 6) via apotome fluorescence microscopy. The microscopy images show that the production of the protein is in good agreement with the results of the qRT-PCR analysis of the COL1α1 gene expression (Fig. 6). Since our experiments represent a condition comparable to the first stages of the tumoral disease, when the collagen production could represent a promotion of cancer cell growth, the COL1α1 inhibitory effect mediated by the CD-SN38 hybrid material demonstrates its superior effect compared to the free SN38.

The study was finally corroborated by the analysis of TGFβ1, a stimulatory cytokine for collagen production participating in the regulation of the tumor growth and microenvironment [35,61,62]. While the TGFβ1 gene expression is maintained at a very low level during the natural cell growth, it was observed overexpression starting at 24 h with CDs, SN38 and CD-SN38 ($p < 0.0001$ for CDs, $p < 0.0001$ for SN38, $p = 0.008$ for CD-SN38), which was maintained only with CDs ($p = 0.0009$ at 48 h, $p.0.006$ at 72 h) confirming the maintaining of COL1α1 overexpression data at 72 h (Figure S23).

4. Conclusions

In summary, we have reported a covalent hybrid material comprising SN38 and CDs (CD-SN38) for the *in vitro* treatment of CRC. CDs are non-toxic and multifunctional nanoplatforms that act as bioimaging agent and reach the cancer cell nucleus bypassing the TME barrier. The slow and

sustained release of SN38 from the hybrid material promotes a longer-lasting effect of the drug, induces damage of the cytoskeleton and the cell cycle preventing the rebound effect on proliferation, and produces a deregulation of the ECM essential components of the tumor niche contrasting the cancer cell growth and reproduction. Additionally, SN38 is tethered onto the surface of CDs via an acid-labile linkage that allows for a controlled release in response to acidic pH, providing a mean of minimizing the amounts of drug released in the circulation (pH 7.4) and targeting release in the nucleus (pH 5.3) of the cancer cells. Future efforts for targeted therapy of chronic diseases characterized by altered ECM deposition, such as chronic kidney disease and chronic allograft nephropathy in kidney transplant patients, are envisaged. This work demonstrates that CDs are promising multifunctional nanocarrier for the efficient bioimaging and delivery of the hydrophobic SN38 drug and points at future interesting developments of water-soluble and dye-doped CDs, synthesized via bottom-up approaches, in the field of cancer treatment.

Data statement

The authors declare that the data supporting the findings of this study are available in the article and its Supplementary Data file. Additional data are available from the corresponding authors upon request.

Credit author statement

D.M., **M.C.**, **F.A.**, **P.M.**, **M.P.** conceived the research and wrote the manuscript. **D.M.** and **M.C.** contributed to experimental design. **D.M.** was responsible of data curation, methodology and cell culture. **M.C.** synthesized and characterized the materials. **M.I.** carried out the gene expression studies. **S.A.** carried out the cytotoxicity test and immunofluorescence experiments. **C.M.A.** was responsible for the statistical analysis. **G.C.** contributed to the technical imaging support. **M.B.** was responsible for the apoptosis and necrosis experiments. **P.M.** and **M.P.** secured the funding. All the authors approved the manuscript.

Declaration of competing interest

The authors declare that they have no known competing financial interests or personal relationships that could have appeared to influence the work reported in this paper.

Acknowledgements

M.P. is the AXA Chair for Bionanotechnology (2016–2023). The authors gratefully acknowledge the financial support from the European Research Council (ERC AdG-2019 n° 885323, e-DOTS), the Spanish Ministerio de Ciencia, Innovación y Universidades (project PID2019-108523RB-I00), IRCCS Ospedale Maggiore Policlinico, the University of Trieste, INSTM, Italian Ministry of Education MIUR (cofin Prot. 2017PBXPN4) and the Maria de Maeztu Units of Excellence Program from the Spanish State Research Agency (Grant No. MDM-2017-0720). The authors thank Dr. Luka Đorđević for fruitful discussions.

Appendix A. Supplementary data

Supplementary data to this article can be found online at https://doi.org/10.1016/j.mtbio.2022.100286.

References

[1] F.T. Kolligs, Diagnostics and epidemiology of colorectal cancer, Vis. Med. 32 (2016) 158–164, https://doi.org/10.1159/000446488.
[2] I. Mármol, C. Sánchez-de-Diego, A.P. Dieste, E. Cerrada, M.J.R. Yoldi, Colorectal carcinoma: a general overview and future perspectives in colorectal cancer, Int. J. Mol. Sci. 18 (2017), https://doi.org/10.3390/ijms18010197.
[3] C. Bailly, Irinotecan: 25 years of cancer treatment, Pharmacol. Res. 148 (2019), https://doi.org/10.1016/j.phrs.2019.104398.
[4] Y.H. Hsiang, L.F. Liu, Identification of mammalian dna topoisomerase i as an intracellular target of the anticancer drug camptothecin, Cancer Res. 48 (1988) 1722–1726.
[5] L.P. Rivory, M.R. Bowles, J. Robert, S.M. Pond, Conversion of irinotecan (CPT-11) to its active metabolite, 7-ethyl-10-hydroxycamptothecin (SN-38) by human liver carboxylesterase, Biochem. Pharmacol. 52 (1996) 1103–1111, https://doi.org/10.1016/0006-2952(96)00457-1.
[6] J.G. Slatter, L.J. Schaaf, J.P. Sams, K.L. Feenstra, M.G. Johnson, P.A. Bombardt, K.S. Cathcart, M.T. Verburg, L.K. Pearson, L.D. Compton, L.L. Miller, D.S. Baker, C.V. Pesheck, R.S. Lord, Pharmacokinetics, metabolism, and excretion of irinotecan (CPT-11) following i.v. infusion of [14C]CPT-11 in cancer patients, Drug Metab. Dispos. 28 (2000) 423–433.
[7] S. Palakurthi, Challenges in SN38 drug delivery: current success and future directions, Expet Opin. Drug Deliv. 12 (2015) 1911–1921, https://doi.org/10.1517/17425247.2015.1070142.
[8] V. Bala, S. Rao, B.J. Boyd, C.A. Prestidge, Prodrug and nanomedicine approaches for the delivery of the camptothecin analogue SN38, J. Contr. Release 172 (2013) 48–61, https://doi.org/10.1016/j.jconrel.2013.07.022.
[9] A. Casadó, M.L. Sagristá, M. Mora, A novel microfluidic liposomal formulation for the delivery of the SN-38 camptothecin: characterization and in vitro assessment of its cytotoxic effect on two tumor cell lines, Int. J. Nanomed. 13 (2018) 5301–5320, https://doi.org/10.2147/IJN.S166219.
[10] D.A. Proia, D.L. Smith, J. Zhang, J.-P. Jimenez, J. Sang, L.S. Ogawa, M. Sequeira, J. Acquaviva, S. He, C. Zhang, V. Khazak, I. Astsaturov, T. Inoue, N. Tatsuta, S. Osman, R.C. Bates, D. Chimmanamada, W. Ying, HSP90 inhibitor–SN-38 conjugate strategy for targeted delivery of topoisomerase I inhibitor to tumors, Mol. Cancer Therapeut. 14 (2015) 2422–2432, https://doi.org/10.1158/1535-7163.MCT-15-0455.
[11] R.M. Sharkey, W.J. McBride, T.M. Cardillo, S.V. Govindan, Y. Wang, E.A. Rossi, C.H. Chang, D.M. Goldenberg, Enhanced delivery of SN-38 to human tumor xenografts with an anti-trop-2–SN-38 antibody conjugate (sacituzumab govitecan), Clin. Cancer Res. 21 (2015) 5131–5138, https://doi.org/10.1158/1078-0432.CCR-15-0670.
[12] M. Bar-Zeev, D. Kelmansky, Y.G. Assaraf, Y.D. Livney, β-Casein micelles for oral delivery of SN-38 and elacridar to overcome BCRP-mediated multidrug resistance in gastric cancer, Eur. J. Pharm. Biopharm. 133 (2018) 240–249, https://doi.org/10.1016/j.ejpb.2018.10.018.
[13] E. Einafshar, A. Haghighi Asl, A. Hasheminia, A. Malekzadeh, M. Ramezani, Synthesis of new biodegradable nanocarriers for SN38 delivery and synergistic phototherapy, Nanomed. J. 5 (2018) 210–216, https://doi.org/10.22038/NMJ.2018.05.00004.
[14] P. Ebrahimnejad, R. Dinarvand, A. Sajadi, M.R. Jaafari, A.R. Nomani, E. Azizi, M. Rad-Malekshahi, F. Atyabi, Preparation and in vitro evaluation of actively targetable nanoparticles for SN-38 delivery against HT-29 cell lines, Nanomed. Nanotechnol. Biol. Med. 6 (2010) 478–485, https://doi.org/10.1016/j.nano.2009.10.003.
[15] F. Nguyen, I. Alferiev, P. Guan, D.T. Guerrero, V. Kolla, G.S. Moorthy, M. Chorny, G.M. Brodeur, Enhanced intratumoral delivery of SN38 as a tocopherol oxyacetate prodrug using nanoparticles in a neuroblastoma xenograft model, Clin. Cancer Res. 24 (2018) 2585–2593, https://doi.org/10.1158/1078-0432.CCR-17-3811.
[16] Z. Liu, J.T. Robinson, X. Sun, H. Dai, PEGylated nanographene oxide for delivery of water-insoluble cancer drugs, J. Am. Chem. Soc. 130 (2008) 10876–10877, https://doi.org/10.1021/ja803688x.
[17] J. Chen, G.M. He, G.Y. Xian, X.Q. Su, L.L. Yu, F. Yao, Mechanistic biosynthesis of SN-38 coated reduced graphene oxide sheets for photothermal treatment and care of patients with gastric cancer, J. Photochem. Photobiol. B Biol. 204 (2020) 111736, https://doi.org/10.1016/j.jphotobiol.2019.111736.
[18] L. Đorđević, F. Arcudi, M. Cacioppo, M. Prato, A multifunctional chemical toolbox to engineer carbon dots for biomedical and energy applications, Nat. Nanotechnol. 17 (2022) 112–130, https://doi.org/10.1038/s41565-021-01051-7.
[19] S.N. Baker, G.A. Baker, Luminescent carbon nanodots: emergent nanolights, Angew. Chem. Int. Ed. 49 (2010) 6726–6744, https://doi.org/10.1002/anie.200906623.
[20] Y.J. Chung, J. Kim, C.B. Park, Photonic carbon dots as an emerging nanoagent for biomedical and healthcare applications, ACS Nano 14 (2020) 6470–6497, https://doi.org/10.1021/acsnano.0c02114.
[21] J. Liu, R. Li, B. Yang, Carbon dots: a new type of carbon-based nanomaterial with wide applications, ACS Cent. Sci. 6 (2020) 2179–2195, https://doi.org/10.1021/acscentsci.0c01306.
[22] W. Pang, P. Jiang, S. Ding, Z. Bao, N. Wang, H. Wang, J. Qu, D. Wang, B. Gu, X. Wei, Nucleolus-targeted photodynamic anticancer therapy using renal-clearable carbon dots, Adv. Healthc. Mater. 9 (2020), https://doi.org/10.1002/ADHM.202000607.
[23] D.K. Ji, H. Dali, S. Guo, S. Malaganahally, J. Vollaire, V. Josserand, H. Dumortier, C. Ménard-Moyon, A. Bianco, Multifunctional carbon nanodots: enhanced near-infrared photosensitizing, photothermal activity, and body clearance, Small Sci 2 (2022) 2100082, https://doi.org/10.1002/smsc.202100082.
[24] M. Ashrafizadeh, R. Mohammadinejad, S.K. Kailasa, Z. Ahmadi, E.G. Afshar, A. Pardakhty, Carbon dots as versatile nanoarchitectures for the treatment of neurological disorders and their theranostic applications: a review, Adv. Colloid Interface Sci. 278 (2020) 102123, https://doi.org/10.1016/J.CIS.2020.102123.
[25] L.M.T. Phan, A.R. Gul, T.N. Le, M.W. Kim, S.K. Kailasa, K.T. Oh, T.J. Park, One-pot synthesis of carbon dots with intrinsic folic acid for synergistic imaging-guided photothermal therapy of prostate cancer cells, Biomater. Sci. 7 (2019) 5187–5196, https://doi.org/10.1039/C9BM01228A.

[26] S.K. Kailasa, D.J. Joshi, M.R. Kateshiya, J.R. Koduru, N.I. Malek, Review on the biomedical and sensing applications of nanomaterial-incorporated hydrogels, Mater. Today Chem. 23 (2022) 100746, https://doi.org/10.1016/j.mtchem.2021.100746.
[27] H. Li, X. Yan, D. Kong, R. Jin, C. Sun, D. Du, Y. Lin, G. Lu, Recent advances in carbon dots for bioimaging applications, Nanoscale Horiz 5 (2020) 218–234, https://doi.org/10.1039/C9NH00476A.
[28] S.L. Gawali, K.C. Barick, N.G. Shetake, V. Rajan, B.N. Pandey, N.N. Kumar, K.I. Priyadarsini, P.A. Hassan, PH-labile magnetic nanocarriers for intracellular drug delivery to tumor cells, ACS Omega 4 (2019) 11728–11736, https://doi.org/10.1021/acsomega.9b01062.
[29] E. Cohen, I. Ophir, Y.B. Shaul, Induced differentiation in HT29, a human colon adenocarcinoma cell line, J. Cell Sci. 112 (1999) 2657–2666, https://doi.org/10.1242/jcs.112.16.2657.
[30] S. Gout, C. Marie, M. Lainé, G. Tavernier, M.R. Block, M. Jacquier-Sarlin, Early enterocytic differentiation of HT-29 cells: biochemical changes and strength increases of adherens junctions, Exp. Cell Res. 299 (2004) 498–510, https://doi.org/10.1016/j.yexcr.2004.06.008.
[31] R.P. Fisher, Secrets of a double agent: CDK7 in cell-cycle control and transcription, J. Cell Sci. 118 (2005) 5171–5180, https://doi.org/10.1242/jcs.02718.
[32] M. Sobecki, K. Mrouj, A. Camasses, N. Parisis, E. Nicolas, D. Llères, F. Gerbe, S. Prieto, L. Krasinska, A. David, M. Eguren, M.C. Birling, S. Urbach, S. Hem, J. Déjardin, M. Malumbres, P. Jay, V. Dulic, D.L. Lafontaine, R. Feil, D. Fisher, The cell proliferation antigen Ki-67 organises heterochromatin, Elife 5 (2016), https://doi.org/10.7554/ELIFE.13722.
[33] M. Huch, E.L. Rawlins, Cancer: tumours build their niche, Nature 545 (2017) 292–293, https://doi.org/10.1038/nature22494.
[34] L. Wang, J. Yu, J. Ni, X.-M. Xu, J. Wang, H. Ning, X.-F. Pei, J. Chen, S. Yang, C.B. Underhill, L. Liu, J. Liekens, J. Merregaert, L. Zhang, Extracellular matrix protein 1 (ECM1) is over-expressed in malignant epithelial tumors, Cancer Lett. 200 (2003) 57–67, https://doi.org/10.1016/S0304-3835(03)00350-1.
[35] B. Costanza, I. Umelo, J. Bellier, V. Castronovo, A. Turtoi, Stromal modulators of TGF-β in cancer, J. Clin. Med. 6 (2017) 7, https://doi.org/10.3390/jcm6010007.
[36] S. Crotti, M. Piccoli, F. Rizzolio, A. Giordano, D. Nitti, M. Agostini, Extracellular matrix and colorectal cancer: how surrounding microenvironment affects cancer cell behavior? J. Cell. Physiol. 232 (2017) 967–975, https://doi.org/10.1002/jcp.25658.
[37] F. Arcudi, L. Đorđević, S. Rebeccani, M. Cacioppo, A. Zanut, G. Valenti, F. Paolucci, M. Prato, Lighting up the electrochemiluminescence of carbon dots through pre- and post-synthetic design, Adv. Sci. 8 (2021) 2100125, https://doi.org/10.1002/advs.202100125.
[38] S. V. Govindan, D.M. Goldenberg, Dosages of Immunoconjugates of Antibodies and SN-38 for Improved Efficacy and Decreased Toxicity for Treatment of Cancers. US20170014403A1, 2017.
[39] F. Arcudi, L. Đorđević, M. Prato, Design, synthesis, and functionalization strategies of tailored carbon nanodots, Acc. Chem. Res. 52 (2019) 2070–2079, https://doi.org/10.1021/acs.accounts.9b00249.
[40] M. Cacioppo, T. Scharl, L. Đorđević, A. Cadranel, F. Arcudi, D.M. Guldi, M. Prato, Symmetry-breaking charge-transfer chromophore interactions supported by carbon nanodots, Angew. Chem. Int. Ed. 59 (2021) 12779–12784, https://doi.org/10.1002/anie.202004638.
[41] L. Đorđević, P. Haines, M. Cacioppo, F. Arcudi, T. Scharl, A. Cadranel, D.M. Guldi, M. Prato, Synthesis and excited state processes of arrays containing amine-rich carbon dots and unsymmetrical rylene diimides, Mater. Chem. Front. 4 (2020) 3640–3648, https://doi.org/10.1039/D0QM00407C.
[42] F. Arcudi, L. Đorđević, M. Prato, Rationally designed carbon nanodots towards pure white-light emission, Angew. Chem. Int. Ed. 56 (2017) 4170–4173, https://doi.org/10.1002/anie.201612160.
[43] F. Arcudi, D.E. Westmoreland, E.A. Weiss, Colloidally stable CdS quantum dots in water with electrostatically stabilized weak-binding, sulfur-free ligands, Chem. Eur J. 25 (2019) 14469–14474, https://doi.org/10.1002/chem.201903908.
[44] N. Sanna, G. Chillemi, L. Gontrani, A. Grandi, G. Mancini, S. Castelli, G. Zagotto, C. Zazza, V. Barone, A. Desideri, UV-vis spectra of the anticancer campothecin family drugs in aqueous solution: specific spectroscopic signatures unraveled by a combined computational and experimental study, J. Phys. Chem. B 113 (2009) 5369–5375, https://doi.org/10.1021/jp809801y.
[45] A.K. Ghosh, M. Brindisi, Organic carbamates in drug design and medicinal Chemistry, J. Med. Chem. 58 (2015) 2895–2940, https://doi.org/10.1021/jm501371s.
[46] T.L. Riss, R.A. Moravec, A.L. Niles, S. Duellman, H.A. Benink, T.J. Worzella, Cell Viability Assays, 2004.
[47] Q. Jia, Z. Zhao, K. Liang, F. Nan, Y. Li, J. Wang, J. Ge, P. Wang, Recent advances and prospects of carbon dots in cancer nanotheranostics, Mater. Chem. Front. 4 (2020) 449–471, https://doi.org/10.1039/C9QM00667B.
[48] E. Henke, R. Nandigama, S. Ergün, Extracellular matrix in the tumor microenvironment and its impact on cancer therapy, Front. Mol. Biosci. (2020) 160, https://doi.org/10.3389/fmolb.2019.00160.
[49] S. Kalan, R. Amat, M.M. Schachter, N. Kwiatkowski, B.J. Abraham, Y. Liang, T. Zhang, C.M. Olson, S. Larochelle, R.A. Young, N.S. Gray, R.P. Fisher, Activation of the p53 transcriptional program sensitizes cancer cells to Cdk7 inhibitors, Cell Rep. 21 (2017) 467–481, https://doi.org/10.1016/j.celrep.2017.09.056.
[50] N. Kwiatkowski, T. Zhang, P.B. Rahl, B.J. Abraham, J. Reddy, S.B. Ficarro, A. Dastur, A. Amzallag, S. Ramaswamy, B. Tesar, C.E. Jenkins, N.M. Hannett, D. McMillin, T. Sanda, T. Sim, N.D. Kim, T. Look, C.S. Mitsiades, A.P. Weng, J.R. Brown, C.H. Benes, J.A. Marto, R.A. Young, N.S. Gray, Targeting transcription regulation in cancer with a covalent CDK7 inhibitor, Nature 511 (2014) 616–620, https://doi.org/10.1038/nature13393.
[51] H. Hong, Y. Zeng, W. Jian, L. Li, L. Lin, Y. Mo, M. Liu, S. Fang, Y. Xia, CDK7 inhibition suppresses rheumatoid arthritis inflammation via blockage of NF-κB activation and IL-1β/IL-6 secretion, J. Cell Mol. Med. 22 (2018) 1292–1301, https://doi.org/10.1111/jcmm.13414.
[52] Y. Xia, L.Y. Lin, M.L. Liu, Z. Wang, H.H. Hong, X.G. Guo, G.Q. Gao, Selective inhibition of CDK7 ameliorates experimental arthritis in mice, Clin. Exp. Med. 15 (2014) 269–275, https://doi.org/10.1007/S10238-014-0305-6.
[53] M. Takagi, T. Ono, T. Natsume, C. Sakamoto, M. Nakao, N. Saitoh, M.T. Kanemaki, T. Hirano, N. Imamoto, Ki-67 and condensins support the integrity of mitotic chromosomes through distinct mechanisms, J. Cell Sci. 131 (2018), https://doi.org/10.1242/jcs.212092.
[54] C.L. Hitchcock, Ki-67 staining as a means to simplify analysis of tumor cell proliferation, Am. J. Clin. Pathol. 96 (1991) 444–446, https://doi.org/10.1093/ajcp/96.4.444.
[55] D. Gisselsson, U. Håkanson, P. Stoller, D. Marti, Y. Jin, A.H. Rosengren, Y. Stewénius, F. Kahl, I. Panagopoulos, When the genome plays dice: circumvention of the spindle assembly checkpoint and near-random chromosome segregation in multipolar cancer cell mitoses, PLoS One 3 (2008), e1871, https://doi.org/10.1371/journal.pone.0001871.
[56] E. Therman, S. Timonen, Multipolar spindles in human cancer cells, Hereditas 36 (2010) 393–405, https://doi.org/10.1111/j.1601-5223.1950.tb03385.x.
[57] R. Ren, H. Sun, C. Ma, J. Liu, H. Wang, Colon cancer cells secrete exosomes to promote self-proliferation by shortening mitosis duration and activation of STAT3 in a hypoxic environment, Cell Biosci. 9 (2019), https://doi.org/10.1186/S13578-019-0325-8.
[58] S. He, Y. Liang, F. Shao, X. Wang, Toll-like receptors activate programmed necrosis in macrophages through a receptor-interacting kinase-3-mediated pathway, Proc. Natl. Acad. Sci. Unit. States Am. 108 (2011) 20054–20059, https://doi.org/10.1073/PNAS.1116302108.
[59] A.G. Porter, R.U. Jänicke, Emerging roles of caspase-3 in apoptosis, Cell Death Differ. 6 (1999) 99–104, https://doi.org/10.1038/sj.cdd.4400476.
[60] L. Wang, J. Yu, J. Ni, X.M. Xu, J. Wang, H. Ning, X.F. Pei, J. Chen, S. Yang, C.B. Underhill, L. Liu, J. Liekens, J. Merregaert, L. Zhang, Extracellular matrix protein 1 (ECM1) is over-expressed in malignant epithelial tumors, Cancer Lett. 200 (2003) 57–67, https://doi.org/10.1016/S0304-3835(03)00350-1.
[61] S.M. Yun, S.H. Kim, E.H. Kim, The molecular mechanism of transforming growth factor-β signaling for intestinal fibrosis: a mini-review, Front. Pharmacol. 10 (2019) 162, https://doi.org/10.3389/fphar.2019.00162.
[62] J. Luo, X.Q. Chen, P. Li, The role of TGF-β and its receptors in gastrointestinal cancers, Transl. Oncol. 12 (2019) 475, https://doi.org/10.1016/J.TRANON.2018.11.010.